Research Article | Vol. 29, No. 3 / 1 February 2021 / Optics Express 4058
Optics EXPRESS

# Observation of the rotational Doppler shift with spatially incoherent light

ALEXANDER Q. ANDERSON,[1,*] ELIZABETH F. STRONG,[2] BRENDAN M. HEFFERNAN,[3] MARK E. SIEMENS,[4] GREGORY B. RIEKER,[2] AND JULIET T. GOPINATH[1,3]

[1]Department of Electrical, Computer, and Energy Engineering, University of Colorado, Boulder, Colorado 80309, USA
[2]Department of Mechanical Engineering, University of Colorado, Boulder, Colorado 80309, USA
[3]Department of Physics, University of Colorado, Boulder, Colorado 80309, USA
[4]Department of Physics and Astronomy, University of Denver, Denver, Colorado 80308, USA
*alexander.q.anderson@colorado.edu

**Abstract:** The rotational Doppler shift (RDS) is typically measured by illuminating a rotating target with a laser prepared in a simple, known orbital angular momentum (OAM) superposition. We establish theoretically and experimentally that detecting the rotational Doppler shift does not require the incident light to have a well-defined OAM spectrum but instead requires well-defined correlations within the OAM spectrum. We demonstrate measurement of the rotational Doppler shift using spatially incoherent light.



## 1. Introduction

The familiar optical linear Doppler shift is the frequency shift of light arising from relative motion between a source and an observer, effecting a change in the linear momentum of the light. Similarly, the rotational Doppler shift (RDS) describes the frequency shift arising from a relative rotation transverse to the light beam and is proportional to the change in orbital angular momentum of the light [1,2]. Orbital angular momentum (OAM) in light is characterized by helical wavefronts, described by phase $e^{i\ell\phi}$, where $\ell$ is the topological charge and $\phi$ is the azimuthal angle [3]. For a change of $\Delta\ell\hbar$ in the OAM of light scattered from a target rotating with angular frequency of $\Omega$, the magnitude of the rotational Doppler shift [2,4] is

$$\Delta\omega = \Delta\ell\Omega \tag{1}$$

RDS measurements are generally performed with a coherent beam composed of either one OAM mode or a "petal beam" superposition of two conjugate OAM modes ($\pm\ell$). This beam is directed onto the rotating target and a photodetector measures the beat frequency intensity modulations of the reflected light [5–7]. A single OAM mode (Fig. 1(A)) is prepared for heterodyne RDS measurements, in which the scattered illumination beam is interfered with a reference mode. Alternatively, a petal beam of azimuthal fringes (Fig. 1(B)) can be used to measure the RDS without a separate reference beam [5–7].

The RDS has been investigated for measuring instrument vibrations [8], vorticity in fluid flows [9,10], angular velocity and acceleration of remote objects [11–15], and the OAM spectrum of an uncharacterized beam [16]. Typically, all of these applications use a narrow linewidth laser, in part due to the simpler conversion into OAM modes for single wavelength beams [17]. Recently, however, Lavery et al. demonstrated that the rotational Doppler shift is independent of optical frequency and can observed using a supercontinuum white-light source [18]. This result shows that the RDS arises even in temporally incoherent light; however, this experiment and other previous demonstrations of the RDS used spatially coherent laser light.

#415580 https://doi.org/10.1364/OE.415580
Journal © 2021 Received 23 Nov 2020; revised 8 Jan 2021; accepted 12 Jan 2021; published 25 Jan 2021

Optics EXPRESS

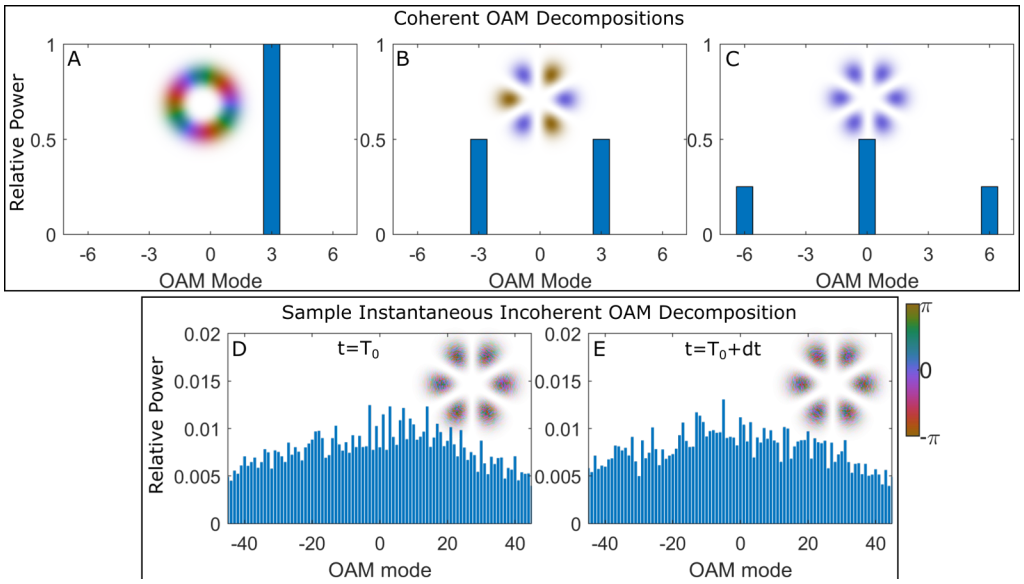


**Fig. 1.** Illustrations of various beams with well-defined OAM superpositions (color is phase and brightness is intensity). (A) A pure OAM mode of $\ell = 3$. (B) A petal beam with equal superpositions of $\ell = 3$ and $\ell = -3$ modes. (C) A "flat" petal beam, composed a complex superposition of OAM modes with consecutive modes separated by $\Delta\ell = 6$. (D, E) Example instantaneous OAM decompositions of incoherent "petal" fields at time $t = T_0$ (D) and $T_0 + dt$ (E).

We show that a spatially incoherent light field (as exemplified in Fig. 1(D)–(E)) can be used to measure rotation rates with the rotational Doppler shift. The ability to measure the RDS from spatially incoherent light presents new rotation sensing applications, including optically-sectioned rotation measurements and passive sensing of rotating astronomical sources [19]. Regardless of the phase profile or even the spatial coherence of the illumination, the measured rotation signal in such an experiment can still be explained as a frequency shift arising from the same rotational Doppler effect.

## 2. Intensity and frequency perspectives on the origin of the RDS

To understand the origin of the rotational Doppler shift, consider a single scatterer rotating about the axis of a spatially coherent incident beam composed of a single OAM mode. The incident electric field is described with an azimuthally varying phase, as

$$E(r, \phi) = E_0(r)e^{i[\omega t - \ell\phi]} \tag{2}$$

where $r$ is the radial coordinate, $\omega$ is the angular optical frequency, and $E_0(r)$ is a function characterizing the radial form of the electric field. Note that we need not specify the particular radial form of the electric field because the RDS is independent of the incident beam's radial distribution, as seen in Eq. (1). A target rotating about the axis of the beam with a constant angular frequency $\Omega$ has an angular position $\phi(t) = \phi_0 + \Omega t$. Because the particle moves along a continuous phase gradient in the light, the phase advances at a rate $\ell\Omega$ faster (or slower, for $\ell$ and $\Omega$ in opposite directions) than the incident field's optical frequency [20]. Thus, the observed electric field has a shifted frequency as seen in Eq. (3).

$$E_{observed} = E_0 e^{i[\omega t - \ell(\phi_0 + \Omega t)]} = E_0 e^{i[(\omega - \ell\Omega)t - \ell\phi_0]} \tag{3}$$

Optics EXPRESS

In order to observe this frequency shift, the scattered light must interfere with a reference beam so that a beat frequency may be measured. Note that this requires careful alignment if a single-valued frequency shift is desired [21].

Illuminating the rotating target with a petal beam composed of conjugate OAM modes, forming azimuthal fringes (Fig. 1(B)), eliminates this alignment step and generates an RDS signal that can be explained equivalently either as an amplitude modulation or as a frequency shift. In the time domain interpretation, a particle rotating about the beam's axis traverses the high and low intensity interference fringes of the petal beam, resulting in an intensity modulation of the scattered light at the detector. Alternatively, this signal may be explained in the frequency domain via the same frequency shift mechanism as the single OAM beam illumination case, applied to each of the two incident $\pm\ell$ OAM modes [4,6]. When these two component modes are scattered into any common detection mode, they each experience a different frequency shift proportional to their respective changes in OAM, resulting in a beat frequency of $2\ell\Omega$ for any mode at the detector.

Most generally, the measured RDS signal is a function of both the OAM modes of the illumination and of the surface characteristics of the rotating target. It is common to represent the spatial distribution of the amplitude and phase of a rotating target as the sum of its topological charges (TCs), $\sum_n A_n(r)e^{in\phi}e^{i\Omega t}$, which corresponds well to the form of the illumination beam composed of a sum of OAM modes, $\sum_m B_m(r)e^{-i\omega t}e^{im\phi}$, where $n$ ($m$) represent the n$^{\text{th}}$- (m$^{\text{th}}$-) order harmonic, and $A_n(r)$ ($B_m(r)$) represent the complex amplitude of the TC [16]. The light scattered from the target may be described as in Eq. (4), where $s$ is the TC of the scattered light:

$$E = \sum_s \sum_m A_{s-m}(r)B_m(r)e^{-i\omega t}e^{is\phi}e^{i(s-m)\Omega t} \tag{4}$$

An individual scattered mode may be selected with a filter if desired. Ignoring the radial functions for simplicity and measuring the power within a single scattered mode yields

$$I_s = \sum_m |B_m A_{s-m}|^2 + 2\sum_{p\le q} |B_p A_{s-p} B_q A_{s-q}| \cos((p-q)\Omega t + \phi_{p,q}) \tag{5}$$

where $\phi_{p,q}$ is the phase of the amplitude term [16]. For a typical measurement using an incident petal beam composed of $\pm\ell$ OAM modes, a single-valued beat frequency may be observed, regardless of whether the rotating target is patterned with a particular set of TCs or if it is randomly structured [4,6,18]; the only requirement of the target is that it contains at least 2 topological charges with a difference of $2\ell$.

This more complete RDS model allows the analysis of more complicated cases, such as petal beams composed of a complex superposition of many OAM modes rather than just $\pm\ell$. Such a petal beam may have the same lobed intensity distribution with a different phase structure (for example, compare the petal beams of Fig. 1(B) and 1(C)); however, the same RDS beat frequency can be observed as in the standard $\pm\ell$ petal illumination case. In this situation, the amplitude modulation model remains an intuitive explanation of the RDS beat, but the frequency shift model requires more consideration: Just as the superposition of several OAM modes interfere to generate a petal beam resulting in a single spatial angular frequency as seen in Fig. 1(C), the beat frequencies between each pair of frequency-shifted modes in the scattered spectrum will sum to a single-valued frequency shift by the rotational Doppler effect. Provided the beam is spatially coherent, a petal beam with any arbitrary phase profile may still be decomposed into a specific superposition of OAM modes, which will result in the same expected RDS signal of $2\ell\Omega$ as expected of a $\pm\ell$ petal beam.

The above analysis assumes that the light is spatially coherent, since an incoherent beam cannot be decomposed into a complex time-independent, superposition of OAM modes (Fig. 1(D)–(E)).

Optics EXPRESS

In the incoherent case, a rotating target experiences the same intensity modulation as it traverses a petal beam, and therefore generates the same signal as the coherent situation. However, the straightforward analysis presented above does not directly answer whether this signal's origin is still due to frequency shifts from the RDS. We demonstrate here that even in the case of a fully incoherent petal field without specific OAM modes, the RDS signal is still observed and fully explained by rotational Doppler effect frequency shifts of the instantaneous OAM modes of the incoherent illumination.

## 3. Theoretical analysis

We now assume a completely spatially incoherent field, such that the correlations in the fields at two locations $\overrightarrow{r_1}$ and $\overrightarrow{r_2}$ approximates a delta function, as described by the mutual coherence function,

$$G(\overrightarrow{r_1}, \overrightarrow{r_2}, \tau) = \langle U(\overrightarrow{r_1}, t) U^*(\overrightarrow{r_2}, t) \rangle = \frac{\bar{\lambda}}{\pi} \delta(\overrightarrow{r_1}, \overrightarrow{r_2}) G(\tau), \tag{6}$$

where $\bar{\lambda}$ is the mean wavelength and $G(\tau)$ is the temporal coherence function for a time delay of $\tau$ [22]

$$G(\tau) = \langle U^*(t) U(t-\tau) \rangle. \tag{7}$$

It has previously been shown that the RDS can be observed with white light [18], so no assumptions of temporal coherence are required. While a spatially incoherent field cannot be represented as a static superposition of modes, the field at time $t_0$ can be decomposed into an instantaneous superposition of modes in any complete basis. In this case, we represent the time varying field in polar coordinates as $f(r, \phi, t)$. A field expressed in Cartesian coordinates may be Fourier transformed to represent the field in a basis of plane waves. Because in polar coordinates, the angular variable $\phi$ is periodic, the field is instead transformed by a Fourier series [23], which allows any arbitrary field to be decomposed into a time-dependent superposition of OAM modes.

$$f(r, \phi, t) = \sum_{\ell=-\infty}^{\infty} f_\ell(r, t) e^{i\ell\phi} \tag{8a}$$

$$f_\ell(r, t) = \frac{1}{2\pi} \int_0^{2\pi} f(r, \phi, t) e^{-i\ell\phi} d\phi \tag{8b}$$

As previously noted, the radial functions for $f_\ell(r, t)$ do not need to be specified, as a full decomposition into specific radial functions is not necessary for this analysis. In general, the OAM spectra will be extremely broad for spatially incoherent light.

Imposing a petal pattern on an incoherent field modifies the field's instantaneous OAM spectrum. A similar effect has been previously demonstrated by Franke-Arnold et al., who showed that passing a beam through an angular aperture introduces OAM to the beam, (however, the mean value of the introduced OAM distribution is zero) [24]. In this work, the field is transmitted through an amplitude mask with a spatial transmission $m(r, \phi)$ matching that of the intensity distribution of a standard $\pm\ell$ petal beam:

$$m(r, \phi) = \cos^2(\ell\phi) m(r) \tag{9}$$

where $m(r)$ is function describing the radial extent of the petals. Just like the electric field, this mask may also be decomposed into its topological charges (TCs) with the same Fourier series notation. When decomposed, the petal mask is seen to contain three TC components:

$$m(r, \phi) = \sum_{n=-\infty}^{\infty} m_n(r) e^{in\phi} = \frac{1}{4} m(r) e^{-i2\ell\phi} + \frac{1}{2} m(r) e^{i0} + \frac{1}{4} m(r) e^{i2\ell\phi} \tag{10}$$

The electric field following the mask, $f'(\vec{r}, t)$, is found by multiplying the mask $m(\vec{r})$ by the incident field $f(\vec{r}, t)$. If both the field and the mask are first decomposed into their OAM

Optics EXPRESS

components, the result is the discrete convolution of the two series [23].

$$f'(\vec{r},t) = f(\vec{r},t)m(\vec{r}) = \sum_{k=-\infty}^{\infty} f'_k(r,t)e^{ik\phi} \tag{11a}$$

$$f'_k(r,t) = f_k * m_k = \sum_{n=-\infty}^{\infty} f_{k-n}(r,t)m_n(r) \tag{11b}$$

$$f'_k(r,t) = \left(\frac{1}{4}f_{k-2\ell}(r,t) + \frac{1}{2}f_k(r,t) + \frac{1}{4}f_{k+2\ell}(r,t)\right)m(r) \tag{11c}$$

This convolution creates three copies of the instantaneous OAM spectrum of the incoherent light, up-shifting one copy in OAM by $+2\ell$ and down-shifting one copy by $-2\ell$, as seen in Eq. (11c) and illustrated in Fig. 2(A)–(B). Although the OAM spectrum is still time-varying and remains broad, the petal mask generates correlations between OAM modes separated by $2\ell$. In other words, for an optical field with a lobed intensity of $N$ petals, the electric field must contain correlations between all pairs of OAM states that satisfy the condition of $\Delta\ell = N$ [25].

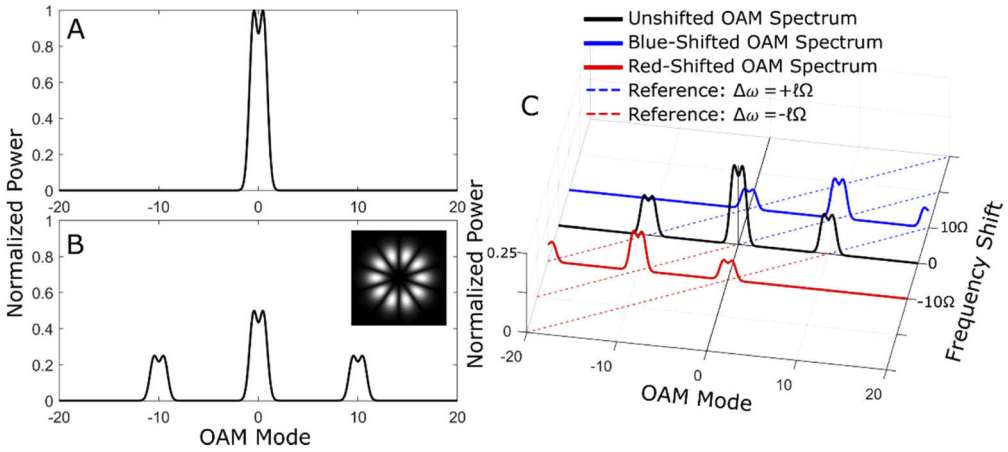


**Fig. 2.** (A) Schematic representation of the instantaneous OAM spectrum of an incoherent, unpatterned, field. (An incoherent OAM spectrum would be quite broad but is shown as above to illustrate the RDS). (B) OAM spectrum of the incoherent field following a static petal mask (inset, $\ell = \pm 5$). The initial spectrum of (A) is copied and shifted by $-2\ell$, 0, and $2\ell$. (C) OAM shifted and frequency shifted spectrum after scattering from a rotating target. In this case, the rotating target's reflectivity had the same topological charges as the incident illumination, so there are only 3 discrete frequency-shifted spectra.

To measure a target's rotation, the incoherent petal field is imaged onto a rotating target with a spatially-varying reflectivity, and this target is imaged onto a photodetector. Like the incident field and the petal mask, the rotating target may also be decomposed into a complex superposition of TCs, with a time-dependent phase on each TC due to the rotation of the target. The reflectivity of the target may of course be designed as various different structures, including simulating one or multiple random particles [5,7]; however, the strongest signals arise from targets patterned with the same TCs as the incident illumination, as this maximizes the overlap integral between the target and the illumination [12]. Only the TCs common to both the target and the illumination mask contribute to the RDS signal; all other topological charges contribute only to DC and shot noise. One of the simplest targets to analyze is one with sinusoidal variation in the reflectivity which matches the angular structure of the incident petal field of Eq. (10). Such a reflectivity pattern, as described by Eq. (12), has the same three components as the petal mask, but with the

Optics EXPRESS

addition of a time and OAM dependent phase, as shown in Eq. (12).

$$R_T(\phi, t) = \cos^2(\ell(\phi + \Omega t)) = \frac{1}{4}e^{-i2\ell\Omega t}e^{-i2\ell\phi} + \frac{1}{2}e^{i0} + \frac{1}{4}e^{i2\ell\Omega t}e^{i2\ell\phi} \tag{12}$$

The application of this rotating mask again results in convolving its TC components with the incident OAM spectrum. In this convolution, the incident OAM spectrum is not only shifted in OAM, but also shifted in frequency proportionally to the change in OAM and the angular frequency $\Omega$, as described by the rotational Doppler effect.

The RDS signal can be measured by imaging the rotating target onto a square-law photodetector, which integrates over the entire image. Because OAM modes are orthogonal and thus dissimilar modes cannot beat, the total signal, $h(t)$, is the sum of the intensity signals $h_k(t)$ from each individual OAM mode at the detector, $g_k(t)$.

$$h(t) = \sum_{k=-\infty}^{\infty} h_k(t) \tag{13a}$$

$$h_k(t) = \int_0^R |g_k(r,t)|^2 \, dr \tag{13b}$$

$$g_k(r,t) = (R_T(t))_k * f_k'(r,t) \tag{13c}$$

$$h_k(t) = \sum_{q=-2}^{2}\sum_{n=-2}^{2}(A_{q,n} + B_{q,n}\cos(\Delta\ell\Omega t) + C_{q,n}\cos(2\Delta\ell\Omega t))\int_0^R m(r) f_{k+q\Delta\ell}(r,\ t) f^*_{k+n\Delta\ell}(r,t)dr \tag{13d}$$

The $A$, $B$, and $C$ coefficients of Eq. (13d) are constants determined by the convolution of the illumination mask $m(\phi)$ and the target's reflectivity $R_T(\phi)$. When light originating in a common OAM mode within the incoherent spectrum [Fig. 2(A)] is shifted into a superposition of OAM modes by the stationary illumination mask [Fig. 2(B)], a rotating target shifts the incident light in this superposition proportionally in both OAM and frequency [Fig. 2(C)], such that light scattered into each common mode may generate beat frequencies. In Fig. 2(C), the beat frequencies generated are seen as the separation between the red-shifted, unshifted (black), and blue-shifted spectra. Therefore, as shown in Eq. (13d), a beat frequency in the k$^{\text{th}}$ OAM mode, $h_k(t)$, is in phase with the beat in all other OAM modes, regardless of the instantaneous modal superposition of the initial incoherent field. while Eq. (13d) and Fig. 2(c) assume the rotating target has a lobed reflectivity with only three TC components, a target with more TCs, such as an azimuthal square wave target, would result in a similar behavior, but with additional shifted copies of the spectrum and the associated additional harmonics of the primary $2\ell\Omega$ beat frequency.

This analysis outlines the model by which the signal from an incoherent petal field may be interpreted as a frequency shift due to the rotational Doppler shift acting on each instantaneous mode. Additionally, this model and the associated experiment demonstrate that the RDS does not require preparation of the incident beam in a specific OAM superposition, but rather only requires known correlations within the instantaneous OAM spectrum, provided that the rotating target contains TCs matching those correlations.

## 4. Experimental results

As a demonstration of the RDS with incoherent light, we designed an experiment which uses an incoherent "petal" field to measure the rotation of a patterned target. Since the experiment does not have a requirement on the temporal coherence $G(\tau)$, the incoherent field may be generated by a temporally incoherent, extended source such as an incandescent lamp. This incoherent field cannot be properly shaped and propagated as a petal beam using a hologram. Instead, a lobed intensity pattern of $N$ petals (matching a petal beam of $\pm N/2$ OAM modes) is formed using a projector (Epson EMP83) and the image of that petal pattern is relayed to a reflective rotating target (Fig. 3). The target is a diffuse reflector masked such that its reflectivity has $N_{target}$-fold

Optics EXPRESS

rotational symmetry and is rotated at an angular frequency of Ω. The light reflected from this target is then imaged onto a large area photodetector (Thorlabs Det36a) and the power spectral density (PSD) of the resulting time-dependent signal is calculated (Fig. 4(A)–(B)). Because the projector produces stationary noise with distinct low frequency peaks, we measured the background PSD to use as a filter, multiplying the signal PSD by the inverse of the background PSD; this also sets the noise floor to 0 dB.

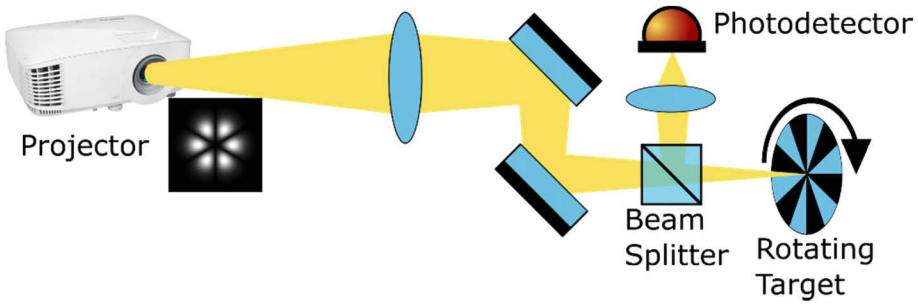


**Fig. 3.** Schematic of incoherent rotational Doppler shift measurement. A projector generates an incoherent image of a "petalled" field with azimuthal fringes (inset). This field is imaged onto a spinning target. The reflectivity of the target is patterned with a specified $N$-fold rotational symmetry to match the periodicity of the incident petal field. The reflected light is imaged onto a photodetector.

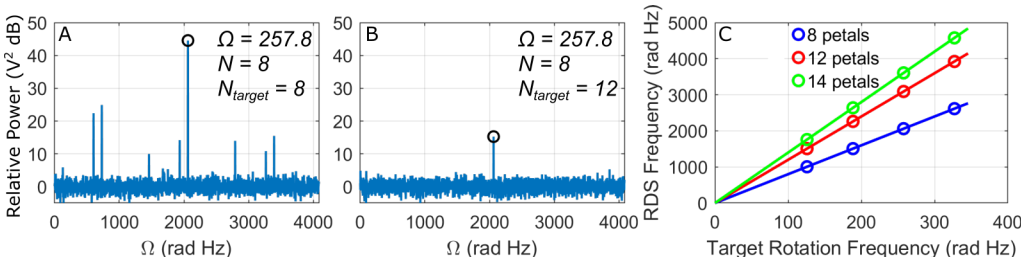


**Fig. 4.** (A, B) Measured power spectral densities, normalized such that the noise floor is at 0 dB. Both use the same 8 petal illumination incident on targets with angular periodicities of (A) $N_{target} = 8$ and (B) $N_{target} = 12$. The expected RDS is marked at 2061rad Hz; the other peaks are due to electronic noise associated with the projector. (C) Observed RDS beat frequency plotted against the target's rotation frequency, for 8, 12, and 14 petal illumination, each measured with a target of matching periodicity. Error bars are smaller than markers—less than 1 rad Hz. Solid lines represent theoretical RDS frequency of $\Delta\ell\Omega$.

Experimental measurements clearly show the expected rotational Doppler shift in the power spectral density at the expected frequency [Fig. 4(A)]. The observed RDS frequency follows the expected linear trend of $N\Omega$ [Fig. 4(C)]. When the rotational symmetry of the target's reflectivity matches that of the illumination, a strong RDS peak is observed in the PSD at $N\Omega$ [Fig. 4(A)]. When the target's reflectivity does not contain the same $N$-fold rotational symmetry as the illumination, no RDS signal is expected, as explained in the previous section. Such a measurement is shown in Fig. 4(B), with illumination of $N = 8$ incident on a target with a rotational symmetry of $N_{target} = 12$; while a small peak is observed, it has 29 dB less power than in the matched case, and we attribute it to an imperfect target mask.

Just as in RDS measurements using coherent laser illumination [4,6,18], the measured RDS peak is seen to scale as $N\Omega$ (Fig. 4(C)). Despite the incoherent OAM spectrum of the illumination,

Optics EXPRESS

a single-valued frequency shift may be measured, as in similar measurements with coherent petal illumination [4,6,18]. The petal mask generates time-independent correlations between all pairs of OAM states that satisfy the condition of $\Delta\ell = N$, and the TCs on the target of 0 and $\pm N_{target}$ measure the presence of these correlations. Since the only correlation present in both the illumination and the target is $\Delta\ell = N$, this is the only RDS harmonic observed.

In contrast to previous RDS measurements, we observe a rotation-dependent frequency shift even when the incident field is incoherent and is not prepared in any particular superposition of OAM modes. Additionally, while the RDS frequency shift arises from the phase gradient associated with the OAM modes, the spatial incoherence of this field dictates that the phase at each location in the field varies on a timescale much faster than the detector's integration time. Despite this fundamental difference, we show that the measurements in this experiment are consistent with a frequency shift due to the rotational Doppler effect. This demonstrates that the RDS does not require the incident field to be prepared with any particular OAM modes.

We have shown that spatially incoherent illumination generates an observable rotational Doppler shift. An RDS signal arises provided that the illumination has well-defined correlations within its OAM spectrum; such OAM correlations are intrinsic to any field with a petal intensity pattern. The spatially incoherent fields analyzed in this discussion must be imaged to the target because unlike coherent Laguerre Gaussian beams, these fields lose their petal structure upon propagation. This means that targets outside the depth of focus of the system return no signal. In applications requiring longitudinal resolution, this may prove advantageous by providing optically sectioned rotation measurements.

**Funding.** National Defense Science and Engineering Graduate; National Science Foundation (DGE 1650115, DMR 1553905, ECCS 1509733, ECCS 1509928, ECCS 1554704); Air Force Office of Scientific Research (FA9550-171-0224); University of Colorado Boulder (Seed Grant Program); Department of Electrical, Computer, and Energy Engineering at University of Colorado Boulder.

**Disclosures.** The authors declare no conflicts of interest.

## References

1. L. Allen, M. Babiker, and W. L. Power, "Azimuthal doppler shift in light beams with orbital angular momentum," Opt. Commun. **112**(3-4), 141–144 (1994).
2. M. J. Padgett, "The mechanism for energy transfer in the rotational frequency shift of a light beam," J. Opt. A: Pure Appl. Opt. **6**(5), S263–S265 (2004).
3. L. Allen, M. W. Beijersbergen, R. J. C. Spreeuw, and J. P. Woerdman, "Orbital angular momentum of light and the transformation of Laguerre-Gaussian laser modes," Phys. Rev. A **45**(11), 8185–8189 (1992).
4. H. Zhou, D. Fu, J. Dong, P. Zhang, and X. Zhang, "Theoretical analysis and experimental verification on optical rotational Doppler effect," Opt. Express **24**(9), 10050 (2016).
5. C. Rosales-Guzmán, N. Hermosa, A. Belmonte, and J. P. Torres, "Experimental detection of transverse particle movement with structured light," Sci. Rep. **3**(1), 2815 (2013).
6. M. P. J. Lavery, F. C. Speirits, S. M. Barnett, and M. J. Padgett, "Detection of a Spinning Object Using Light's Orbital Angular Momentum," Science **341**(6145), 537–540 (2013).
7. A. Q. Anderson, E. F. Strong, B. M. Heffernan, M. E. Siemens, G. B. Rieker, and J. T. Gopinath, "Detection technique effect on rotational Doppler measurements," Opt. Lett. **45**(9), 2636 (2020).
8. S. Xiao, L. Zhang, D. Wei, F. Liu, Y. Zhang, and M. Xiao, "Orbital Angular Momentum-Enhanced Measurement of Rotation Vibration Using a Sagnac Interferometer," Opt. Express **26**(2), 1997–2005 (2018).
9. A. Ryabtsev, S. Pouya, A. Safaripour, M. Koochesfahani, and M. Dantus, "Fluid flow vorticity measurement using laser beams with orbital angular momentum," Opt. Express **24**(11), 11762 (2016).
10. A. Belmonte, C. Rosales-Guzmán, and J. P. Torres, "Measurement of flow vorticity with helical beams of light," Optica **2**(11), 1002 (2015).
11. W. Zhang, J. Gao, D. Zhang, Y. He, T. Xu, R. Fickler, and L. Chen, "Free-Space Remote Sensing of Rotation at the Photon-Counting Level," Phys. Rev. Appl. **10**(4), 044014 (2018).
12. D. B. Phillips, M. P. Lee, F. C. Speirits, S. M. Barnett, S. H. Simpson, M. P. J. Lavery, M. J. Padgett, and G. M. Gibson, "Rotational Doppler velocimetry to probe the angular velocity of spinning microparticles," Phys. Rev. A **90**(1), 011801 (2014).
13. Y. Zhai, S. Fu, J. Zhang, Y. Lv, H. Zhou, and C. Gao, "Remote detection of a rotator based on rotational Doppler effect," Appl. Phys. Express **13**(2), 022012 (2020).
14. Y. Zhai, S. Fu, C. Yin, H. Zhou, and C. Gao, "Detection of angular acceleration based on optical rotational Doppler effect," Opt. Express **27**(11), 15518 (2019).

Optics EXPRESS

15. C. Rosales-Guzmán, N. Hermosa, A. Belmonte, and J. P. Torres, "Measuring the translational and rotational velocities of particles in helical motion using structured light," Opt. Express **22**(13), 16504 (2014).
16. H.-L. Zhou, D.-Z. Fu, J.-J. Dong, P. Zhang, D.-X. Chen, X.-L. Cai, F.-L. Li, and X.-L. Zhang, "Orbital angular momentum complex spectrum analyzer for vortex light based on the rotational Doppler effect," Light: Sci. Appl. **6**(4), e16251 (2017).
17. J. Leach and M. Padgett, "Observation of chromatic effects near a white-light vortex," New J. Phys. **5**, 154 (2003).
18. M. P. J. Lavery, S. M. Barnett, F. C. Speirits, and M. J. Padgett, "Observation of the rotational Doppler shift of a white-light, orbital-angular-momentum-carrying beam backscattered from a rotating body," Optica **1**(1), 1 (2014).
19. R. Neo, S. Leon-Saval, J. Bland-Hawthorn, and G. Molina-Terriza, "OAM interferometry: the detection of the rotational Doppler shift," Opt. Express **25**(18), 21159 (2017).
20. A. Belmonte and J. P. Torres, "Optical Doppler shift with structured light," Opt. Lett. **36**(22), 4437–4439 (2011).
21. M. V. Vasnetsov, V. A. Pas'ko, and M. S. Soskin, "Analysis of orbital angular momentum of a misaligned optical beam," New J. Phys. **7**, 46 (2005).
22. J. W. Goodman, *Statistical Optics* (John Wiley & Sons, Inc., 2015).
23. N. Baddour, "Two-Dimensional Fourier Transforms in Polar Coordinates," in *Advances in Imaging and Electron Physics* (Elsevier, 2011), Vol. 165, pp. 1–45.
24. S. Franke-Arnold, S. M. Barnett, E. Yao, J. Leach, J. Courtial, and M. Padgett, "Uncertainty principle for angular position and angular momentum," New J. Phys. **6**, 103 (2004).
25. N. M. Elias, "Photon orbital angular momentum in astronomy," Astron. Astrophys. **492**(3), 883–922 (2008).